ACS APPLIED MATERIALS & INTERFACES

Research Article

www.acsami.org

ZnO-Reinforced Poly(3-hydroxybutyrate-*co*-3-hydroxyvalerate) Bionanocomposites with Antimicrobial Function for Food Packaging

Ana M. Díez-Pascual*,† and Angel L. Díez-Vicente‡

†Institute of Polymer Science and Technology (ICTP-CSIC), Juan de la Cierva 3, 28006 Madrid, Spain

‡Airbus Operations S. L., John Lennon s/n, 28906 Getafe, Madrid, Spain

ABSTRACT: Biodegradable nanocomposites were prepared by adding ZnO nanoparticles to bacterial polyester poly(3-hydroxybutyrate-*co*-3-hydroxyvalerate) (PHBV) via solution casting technique. The morphology, thermal, mechanical, antibacterial, barrier, and migration properties of the nanocomposites were analyzed. The nanoparticles were uniformly dispersed within PHBV without the aid of coupling agents, and acted effectively as nucleating agents, raising the crystallization temperature and the level of crystallinity of the matrix while decreasing its crystallite size. A gradual rise in thermal stability was found with increasing ZnO loading, since the nanofillers hinder the diffusion of volatiles generated during the decomposition process. The nanocomposites displayed superior stiffness, strength, toughness, and glass transition temperature, whereas they displayed reduced water uptake and oxygen and water vapor permeability compared to the neat biopolymer, related to the strong matrix−nanofiller interfacial adhesion attained via hydrogen bonding interactions. At an optimal concentration of 4.0 wt % ZnO, the tensile strength and Young's and storage moduli showed a maximum that coincided with the highest crystallinity and the best barrier properties. PHBV/ZnO films showed antibacterial activity against human pathogen bacteria, and the effect on *Escherichia coli* was stronger than on *Staphylococcus aureus*. The overall migration levels of the nanocomposites in both nonpolar and polar simulants dropped upon increasing nanoparticle content, and were well below the limits required by the current normative for food packaging materials. These sustainable nanomaterials with antimicrobial function are very promising to be used as containers for beverage and food products as well as for disposable applications like cutlery or overwrap films.

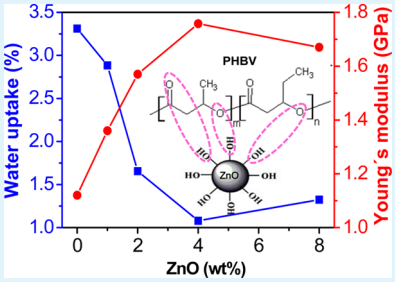

KEYWORDS: *poly(3-hydroxybutyrate-co-3-hydroxyvalerate), ZnO nanoparticles, mechanical performance, antimicrobial activity, barrier properties*

1. INTRODUCTION

Currently, there is growing interest in developing bionanocomposites, that is, composites in which the matrix is a biopolymer and the reinforcements have at least one dimension below 100 nm, in order to replace conventional nonbiodegradable petroleum-based plastic materials that cause harmful effects on the environment, particularly within the field of food packaging applications.[1] Biopolymers or biodegradable plastics are polymeric materials in which at least one step in the degradation process is through metabolism of naturally occurring organisms.[2] Under appropriate conditions of moisture, temperature, and oxygen, biodegradation results in fragmentation or disintegration of the plastics without toxic residue. Among the wide variety of biopolymers that have been studied over the past years, polyhydroxyalkanoates (PHAs) have attracted special interest because of their natural origin. PHAs are a family of completely biodegradable and biocompatible polyesters synthesized by bacterial fermentation from renewable resources like cane sugar. More than 150 different types of PHAs consisting of various monomers have been reported;[3] therefore, the properties of this biopolymer family are very broad, and can be applied in the fields of medicine, agriculture, and packaging. The most widely studied and easiest to produce member of this family is poly(3-hydroxybutyrate) (PHB), an isotactic, high-molecular-weight polyester with physical properties similar to those of polypropylene (PP). This material presents a relatively high melting and glass transition temperature, as well as good stiffness due to its high crystallinity (>50%). However, the use of PHB has been limited due to several drawbacks such as poor impact resistance, relatively high water vapor permeability (WVP) as well as thermal degradation at temperatures not far above the melting point, which results in a narrow processing window. To overcome these shortcomings, PHB homopolymer can be plasticized internally by bacterial fermentation using 3-hydroxyvalerate, 4-hydroxybutyrate, 3-hydroxyhexanoate or 3-hydroxypropionate.[4] In particular, when 3-hydroxyvalerate units are incorporated into PHB to obtain poly(3-hydroxybutyrate-*co*-3-hydroxyvalerate) (PHBV), with a chemical formula of $[COCH_2CH(CH_3)O]_m[COCH_2CH(C_2H_5)O]_n$, the degree of crystallinity, melting and glass transition temperature decrease and the processing window slightly broadens, because these monomers have improved melt stability at low processing temperatures.[5] However, the drop in crystallinity provokes a

Received: April 14, 2014
Accepted: May 20, 2014
Published: May 20, 2014

   dx.doi.org/10.1021/am502261e | *ACS Appl. Mater. Interfaces* 2014, 6, 9822−9834

reduction in stiffness and impairs the barrier properties, which might be a disadvantage for the use of PHBV in packaging applications. With a view to expand its range of practical applications, new approaches are sought like the incorporation of nanofillers such as organically modified montmorillonite (OMMT),[6] multiwalled carbon nanotubes (MWCNTs),[7] graphene oxide (GO),[8] cellulose nanocrystals (CNC),[9] or cellulose nanowhiskers (CNW).[10] Improved mechanical performance and higher thermal and barrier properties have been obtained upon addition of small amounts of nanosized fillers into this biopolymer matrix, albeit the enhancements do not meet the requirements for industrial applications. PHBV nanocomposites can be prepared by several techniques, including solution casting and melt compounding, and it has been demonstrated[10] that solution processed samples exhibit more homogeneous nanofiller dispersion and consequently improved performance in comparison to melt processed ones; therefore, solution casting using chloroform or *N,N*-dimethylformamide (DMF) as solvent is the most common method to process these thermoplastic-based materials.

It is well-known that the incorporation of inorganic nanoparticles is an efficient strategy to enhance the properties of polymeric materials. In particular zinc oxide (ZnO) nanostructures, with their large volume to area ratio, highly crystalline structure, outstanding mechanical properties, low coefficient of thermal expansion and high thermal conductivity, are highly potential candidates to be used as reinforcing fillers in polymer composites. Further, they possess radiation hardness, high ultraviolet absorption, and strong antimicrobial activity in the pH range of 7−8 eV in the absence of light, and hence have been extensively used for applications such as catalysts,[11] gas sensors,[12] optical devices,[13] and antimicrobials.[14] Previous studies have demonstrated that ZnO nanoparticles are very effective for enhancing the mechanical performance and antibacterial properties of polymers such as poly(ether ether ketone) (PEEK),[15,16] polyurethane (PU)[17] and ultrahigh-molecular-weight polyethylene (UHMWPE).[18] These low-cost nanofillers can be synthesized through a variety of techniques including hydrothermal synthesis, thermal evaporation, electrochemical decomposition, sonochemical method, sol−gel, and so forth.[19−21] More importantly, they are considered to be nontoxic and listed by FDA as generally recognized as safe "GRAS" substances, and recent studies have reported that they do not cause any damage to the DNA of human cells.[22] ZnO-reinforced materials are expected to have many applications in daily life, particularly in the field of food packaging.[2] In fact, several authors have demonstrated the suitability of nano-ZnO for use in food systems like fruit juice packages.[23,24] Antimicrobial food packaging composites have to expand the lag phase and reduce the growth rate of microorganisms in order to extend shelf life and preserve the quality and safety of food products during transportation and storage. They should also impede gain or loss of moisture; prevent chemical contamination; and act as a barrier against permeation of water vapor, oxygen, carbon dioxide, and other volatile compounds. In addition, high mechanical strength, good thermal and dimensional stability, recyclability, and biodegradability are highly desirable.[2]

In a previous report, PHBV/ZnO composite nanofibrous membranes were fabricated by an electrospinning method.[25] However, in such study only the morphology and crystallization behavior of the electrospun fibers were investigated. The present article focuses on the preparation and characterization of ZnO-reinforced PHBV nanocomposites via simple solution casting technique. Using this approach, different amounts of ZnO nanoparticles have been successfully incorporated in the biopolymer matrix without the need for surfactants or coupling agents. The influence of the inorganic nanofillers on the morphology, crystallization behavior, thermal stability, mechanical performance, barrier, migration, and antibacterial properties of the resulting bionanocomposites is investigated in detail throughout this work.

2. EXPERIMENTAL SECTION

Materials and Preparation of the Nanocomposites. Poly(3-hydroxybutyrate-*co*-3-hydroxyvalerate) (PHBV) with a HV content of 12 mol % was purchased from Goodfellow Corp. It presents the following physical characteristics: M_n = 84 000 g/mol; $T_g \approx 23$ °C, $T_m \approx 165$ °C, $d_{25\ °C} = 1.25$ g/cm^3, PDI = 2.4. The polymer was dried in an oven at 70 °C for 24 h to remove absorbed moisture. Zinc oxide nanopowder, <100 nm particle size and specific surface area in the range of 15−25 m^2/g, was supplied by Sigma-Aldrich. Chloroform ($CHCl_3$) was also purchased from Sigma-Aldrich and used as received. Pure PHBV films were prepared via solution casting technique using chloroform as solvent. To improve the nanofiller dispersion within the matrix, the nanocomposites containing 1.0, 2.0, 4.0, and 8.0 wt % ZnO were prepared in a two stage process. First, the corresponding amount of ZnO was dispersed in chloroform by ultrasonication for 30 min. Second, the PHBV powder was dissolved at 50 °C in the nanoparticle dispersion and the mixture was then sonicated for another 20 min and subsequently cast onto a glass Petri dish to evaporate the chloroform at room temperature. Finally, the resulting films were dried under vacuum for 48 h to remove the residual solvent.

Characterization Techniques. Scanning electron microscopy (SEM) was conducted on a SU8000 Hitachi microscope applying an acceleration voltage of 2.0 kV. Samples were cryo-fractured in liquid nitrogen and then sputtered with an Au−Pd mixture under vacuum to avoid charge accumulation during electron irradiation. Transmission electron microscopy (TEM) images were obtained with a Philips Tecnai 20 FEG (LaB_6 filament) electron microscope fitted with an EDAX detector operating at 200 kV. Ultrathin sections of the composites were cut using a diamond knife and a Reichert Ultracut-S ultramicrotome equipped with a FCS cryo-device and placed onto copper grids.

The nonisothermal crystallization and melting behavior of the films was characterized by differential scanning calorimetry (DSC) on a Mettler DSC 30 with a TC15 TA controller using N_2 as the purging gas. The sample treatment consisted in a first heating step from 25 to 195 °C, a subsequent cooling down to 25 °C and a second heating stage up to 195 °C. The heating and cooling rate was 10 °C/min and the sample weight was ∼12 mg. The transition temperatures were taken as the peak maximum or minimum in the calorimetric curves. The degree of crystallinity was calculated from the normalized peak enthalpies according to the equation: $X_m = \Delta H_{m,PHBV} / (\Delta H^\circ_{m,PHBV} \times w_{PHBV})$ where $\Delta H_{m,PHBV}$ is the apparent melting enthalpy of PHBV, w_{PHBV} is the weight fraction of PHBV in the composites and $\Delta H^\circ_{m,PHBV}$ is the theoretical value of enthalpy for a 100% crystalline sample (109 J/g).[26]

X-ray diffraction (XRD) patterns were collected with a Bruker D8 Advance diffractometer using a Cu tube as X-ray source (λ CuKα = 1.54 Å), with a voltage of 40 kV and an intensity of 40 mA. The results were analyzed with the fitting software Topas 2.1 in Bragg−Brentano geometry in the angular range of 2θ = 5−40°, with angular increment of 0.05° and accumulation time of 3 s.

The thermal stability was analyzed by thermogravimetric analysis (TGA) with a TA Instruments Q50 thermobalance. The samples (ca. 20 mg) were dried overnight at 50 °C and subsequently heated from room temperature to 550 °C at a rate of 10 °C/min under an inert atmosphere.

Tensile tests were performed according to the ASTM D 638-03 standard[27] on a servo-hydraulic testing machine (type MTS 858)

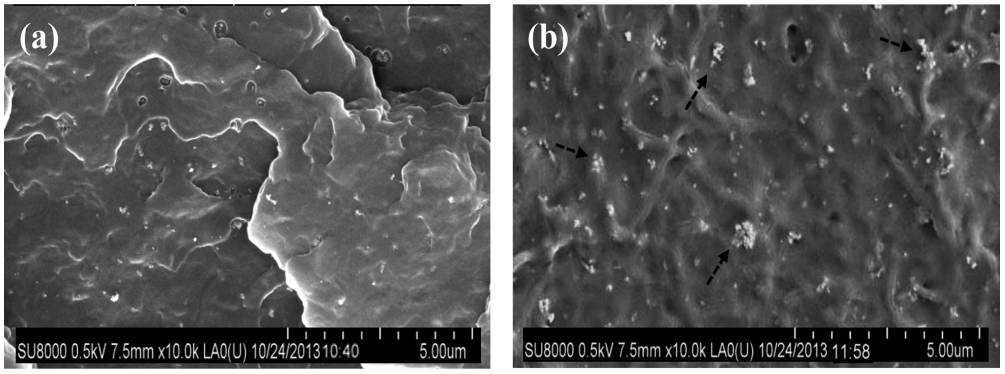

Figure 1. SEM images from fractured surfaces of PHBV/ZnO nanocomposites with (a) 1.0 wt % and (b) 8.0 wt % nanoparticle content. The arrows in b point out small nanoparticle aggregates.

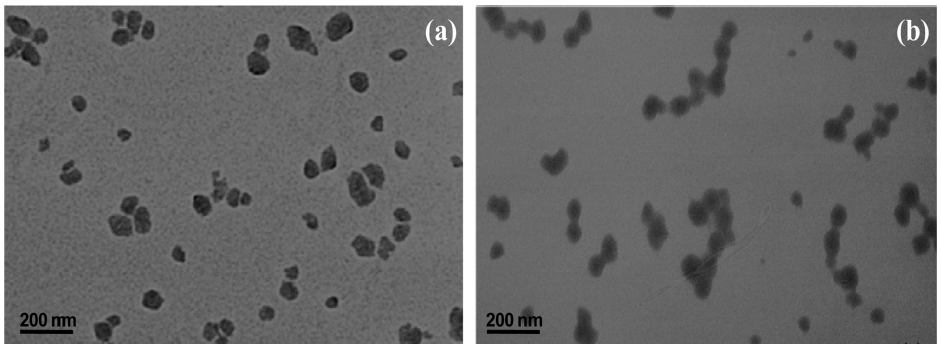

Figure 2. TEM images of PHBV/ZnO nanocomposites with (a) 4.0 wt % and (b) 8.0 wt % ZnO loading.

placed into an environmental chamber at 23 °C and 50% relative humidity (RH), with a crosshead speed of 1 mm/min and a load cell of 100 kN. All the samples were conditioned for 24 h before the measurements. Five specimens for each type of nanocomposite were tested to check for repeatability.

Charpy notched impact strength tests were carried out on a CEAST Fractovis dart impact tester, using a hammer mass that impacted with an energy of 7.10 J on notched specimen bars, according to the ASTM D 6110-10 standard.[28] Measurements were performed at 23 °C and 50% RH. The presented data correspond to the average value of seven test specimens.

The dynamic mechanical performance was analyzed with a Mettler DMA861 dynamic mechanical analyzer. Measurements were carried out in the tensile mode on rectangular shaped bars, in the temperature range between −100 and 100 °C at a heating rate of 2 °C/min and frequency of 1 Hz. Experiments were performed in triplicate to obtain average values.

The antibacterial activity of the composites was tested against two test organisms: Gram-positive *Staphylococcus aureus* (*S. aureus*, ATCC 12600) and Gram-negative *Escherichia coli* (*E. coli*, ATCC 25922). Experiments were carried out without exposure to UV light. All the samples were sterilized in an autoclave prior to the tests, and then submerged in a 3-day-old nutrient broth of ~2.0×10^6 colony forming units per mL (CFU/mL). After incubation at 37 °C for 24 h, the number of viable microorganism colonies was counted manually using a pen and a click-counter, and the results were expressed as mean CFU/sample. The survival ratio (SR) was calculated using the equation: $SR = (N/N_o) \times 100$, where N_o and N are the mean number of bacteria on the pure PHBV and the nanocomposites, respectively. The tests were conducted in triplicate and the average values are reported.

To determine the water absorption, samples were dried in a desiccator at 0% RH for 1 week. Subsequently, they placed in a beaker at 100% RH and allowed to absorb water until a constant weight was attained. Water uptake was calculated as follows: $[(W_f - W_i)/W_i] \times 100$, where W_i and W_f are the initial and final (equilibrium) weight of the samples, respectively. Five replicates for each sample were measured, and the average value is reported.

Water vapor permeability (WVP) was determined at 25 °C following the gravimetric method ASTM E96−95 standard[29] using Payne permeability cups of 3.5 cm diameter. Samples were equilibrated at 54% RH by using magnesium nitrate-6-hydrate. WVP was calculated according to the equation: $WVP = (\Delta m l)/(At\Delta P)$, where Δm is the weight loss of each cup, l the thickness of the film, A the conctact area, t the time, and ΔP the partial pressure difference between inside and outside of the cup. Tests were replicated four times and average values and standard errors are reported.

Oxygen permeability (OP) was evaluated at 25 °C on films equilibrated at 54% RH by measuring the oxygen transference rate (OTR) with a gas permeability tester (Ox-Tran 1/50 System), following the ASTM D3985-05 standard.[30] OP was calculated following the expression: $OP = (OTRl)/\Delta P$, where l is the average film thickness and ΔP the difference between oxygen partial pressure across the film. The results were taken as the average of three tests.

Overall migration tests were performed in two liquid food simulants: ethanol 10% (v/v) and isooctane, according to the EN-1186-1 standard.[31] Nanocomposite films were immersed in a beaker with 10 mL of ethanol and kept in a controlled chamber at 40 °C during 10 days; analogously, samples were immersed in isooctane and maintained at 20 °C for 2 days. Subsequently, the films were removed, the simulants were evaporated and the residue was weighed using a Sartorious 6080 electronic balance (readability of 0.001 mg) in order to determine the overall migration. Experiments were performed in triplicate and average values are reported.

3. RESULTS AND DISCUSSION

Surface Morphology. Typical SEM images from cryo-fractured surfaces of PHBV nanocomposites with 1.0 and 8.0 wt % ZnO are shown in images a and b in Figure 1, respectively. The white dots in the micrographs correspond to the nanoparticles that present quasi-spherical shape and a mean

diameter of 75 nm. A random and very uniform nanofiller dispersion can be observed in the nanocomposite with the lowest ZnO content, without any agglomerates. Similar morphology was found for the nanocomposites incorporating 2.0 or 4.0 wt % ZnO. The interactions between the −OH groups of the ZnO surface and the polar moieties of the biopolymer should prevent nanoparticle aggregation and improve the compatibility between the filler and matrix phases. However, the nanocomposite with 8.0 wt % ZnO displays poorer nanofiller dispersion, with small clusters composed of a few particles. Thus, it was not possible to individually disperse such high ZnO loading, albeit the nanoparticles were on the whole reasonably well distributed throughout the matrix. Interestingly, PHBV/ZnO (1.0 wt %) shows a relatively smooth morphology, whereas that of the nanocomposite with 8.0 wt % ZnO is considerably rougher, a fact that is indicative of a change in the degree of crystallinity of the matrix, as will be shown from DSC analysis.

TEM analysis was also carried out to assess the state of ZnO dispersion within the matrix, and typical micrographs of nanocomposites with 4.0 and 8.0 wt % loading are compared in Figure 2. In the sample with 4.0 wt % ZnO (Figure 2a), the nanoparticles are evenly and well distributed, without forming agglomerates. However, higher amounts of nanoparticles lead to increased propensity toward aggregation (Figure 2b), because the surface hydroxyl groups of ZnO have a strong tendency to create hydrogen bonds, causing the formation of small clusters, in agreement with SEM observations. Overall, SEM and TEM micrographs reveal that ZnO nanoparticles were efficiently dispersed within the biopolymer without the need for surfactants or compatibilizing agents, which confirms the effectiveness of the processing route employed for the preparation of the nanocomposites.

Crystallization and Melting Behavior. It is of great importance and interest to study the crystallization and melting behavior of polymer bionanocomposites since it affects not only the crystalline structure and morphology but also the macroscopic properties of the materials. Therefore, non-isothermal melt crystallization of neat PHBV and its nanocomposites was investigated by DSC analysis, and their first cooling and second heating thermograms are shown in panels a and b in Figure 3, respectively. The thermal parameters derived from DSC curves are collected in Table 1. As can be observed, the crystallization peak temperature (T_p) is about 77 °C for neat PHBV, and shifts progressively toward higher temperature with increasing ZnO concentration, the maximum increase being ∼26 °C for the nanocomposite with the highest loading (inset of Figure 3a). These results point out that the nanoparticles accelerate the crystallization rate of the matrix via heterogeneous nucleation effect. Moreover, the crystallization peak sharpens in the nanocomposites, demonstrating that the homogeneously dispersed ZnO nanofillers effectively act as nucleating agents, thus facilitating the crystallization process of the biopolymer. An analogous nucleating role on PHBV crystallization has been previously reported for other nanofillers like MWCNTs[32] or SiO_2,[33] though the nucleating effect of ZnO nanoparticles is stronger, likely because of their more homogeneous dispersion, and hence a larger number of sites available for nucleation and, as a result, higher crystallization temperature. In contrast, a reduction in T_p has been reported for PHBV nanocomposites reinforced with OMMT[6] or nanofibrillated cellulose (NFC),[34] attributed to compatibility of the nanoclay with the polymer matrix, which

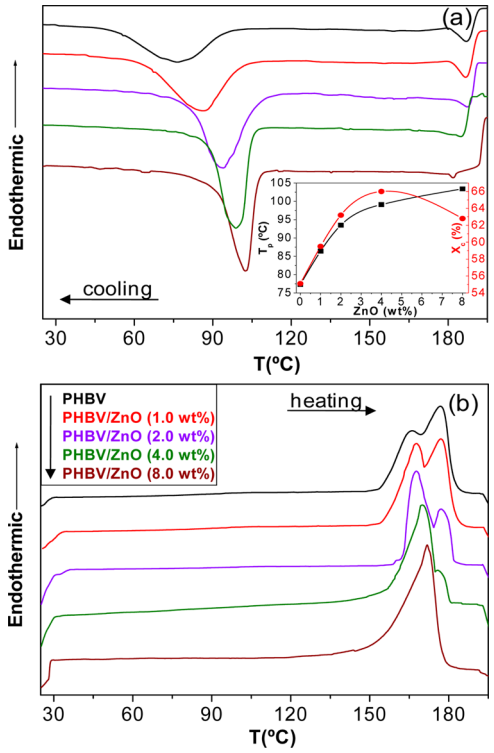

Figure 3. Nonisothermal DSC (a) first cooling and (b) second heating thermograms of PHBV and its nanocomposites at a rate of 10 °C/min. The inset in Figure 2a shows the change in the crystallization peak temperature (T_p) and degree of crystallinity (X_c) vs ZnO concentration.

Table 1. Characteristic Degradation Temperatures and Crystallization and Melting Parameters for PHBV/ZnO Nanocomposites[a]

ZnO (wt %)	T_p (°C)	T_m (°C)	X_c (%)	T_i (°C)	T_{10} (°C)	T_{max} (°C)	CR (%)
0	77.3	165/176	55.1	298.2	322.0	351.3	1.6
1.0	86.4	167/177	59.5	295.4	323.2	363.6	2.4
2.0	93.5	168/177	62.8	308.1	330.5	372.3	3.7
4.0	99.1	170/176s[b]	66.3	319.9	341.4	377.0	4.8
8.0	103.4	171	63.2	317.8	346.8	382.9	8.9

[a] T_p, peak crystallization temperature; T_m, peak melting temperature; X_c, degree of crystallinity; T_i, initial degradation temperature obtained at 2% weight loss; T_{10}, temperature for 10% weight loss; T_{max}, temperature of maximum rate of weight loss; CR, char residue. [b] s, shoulder.

suppressed the crystallization, or polymer degradation through residual moisture in the NFC. Further, in PHBV/ZnO composite nanofibers fabricated by an electrospinning method,[25] the nanoparticles were found to retard the crystallization process of the matrix, likely related to the preferential location of ZnO in certain regions of the fibers; this corroborates the strong influence of the processing method on the state of nanofiller dispersion, location, and orientation within the matrix, hence on the final properties of the nanocomposites. Regarding the level of crystallinity (X_c), the trend is qualitatively similar to that described above for T_p, showing a remarkable increase from ∼55% for the neat matrix to about 66% for the nanocomposite with 4.0 wt % ZnO, whereas it slightly drops to 63% at higher concentration (inset of Figure 3a). In the nanocomposite with 8.0 wt % loading,

although the nanoparticles are on a whole well distributed within the matrix and consequently provide a large nucleation surface, the strong interactions between the hydroxyl groups of the ZnO surface and the C═O of the ester groups of PHBV could hinder the diffusion of the polymer chains and the crystal growth, thereby leading to a fall in X_c. Similar behavior has been described for nanocomposites reinforced with PHBV-grafted-MWCNTs, where the level of crystallinity decreased at nanofiller concentrations >7 wt % because of chain entanglement between the matrix and filler phases that strongly restricted the mobility of the crystalline PHBV segments.[7] These changes in crystallinity have a significant effect on the mechanical performance of the nanocomposites, as will be shown from DMA and tensile tests.

The heating scans obtained after dynamic crystallization are shown in Figure 3b. Neat PHBV displays double melting behavior, in agreement with the results reported previously,[35] which has been usually interpreted in terms of the melting, recrystallization, and remelting model.[36] The first endothermic peak at 165 °C (T_{m1}) arises from the melting of the original crystals formed during the nonisothermal crystallization from the melt at a constant cooling rate, while the second at 176 °C (T_{m2}) corresponds to the melting of crystals formed through recrystallization and reorganization during the DSC heating process. All the nanocomposites except that with 8.0 wt % ZnO also exhibit bimodal melting behavior, showing a gradual increase in T_{m1} with increasing nanofiller loading (by up to 8 °C, Table 1), together with a narrowing of the peak, consistent with the increase in crystallinity found from the cooling thermograms. However, the position of T_{m2} remains merely unchanged upon addition of the nanoparticles. A close analysis of the melting endotherms reveals that T_{m1} peak area is larger for the nanocomposites as compared to that of neat PHBV, whereas the area and height of the T_{m2} peak decrease gradually with increasing ZnO content. A similar phenomenon has been reported by Vidhate et al.[32] and Liu et al.[37] for MWCNT- and layer double hydroxides (LDH)-reinforced PHBV nanocomposites. These authors suggested that the low-temperature melting peak was likely related to heterogeneous nucleation, which started spontaneously by chain aggregation below the melting point, whereas the high-temperature one was ascribed to homogeneous nucleation of the polymer. The smaller area of the second endothermic peak in PHBV/ZnO nanocomposites in comparison to that of the biopolymer points out that ZnO nanoparticles hinder the recrystallization of the matrix crystals, which could be related to the restrictions in chain mobility arising from the strong nanofiller−matrix interactions. An analogous behavior of recrystallization constraint has been previously described for PHBV nanocomposites reinforced with MWCNTs.[32] Nevertheless, the composite with the highest loading presents a single melting peak at about 171 °C. The disappearance of double endothermic peaks provides further evidence for the highly efficient nucleation activity of these inorganic nanoparticles toward enhanced crystallization of PHBV. Consequently, the crystals in the nanocomposites are more perfect and stable than those of the neat biopolymer.

Crystalline Structure. The XRD patterns of neat PHBV, ZnO nanoparticles and the corresponding nanocomposites are shown in Figure 4. The nanoparticles exhibit characteristic peaks at 2θ values of 31.8, 34.4, and 36.2°, arising from the diffraction of the (100), (002), and (101) crystalline planes, respectively, of the hexagonal ZnO wurtzite structure (JCPDS data No. 36−1451). On the other hand, the diffractogram of

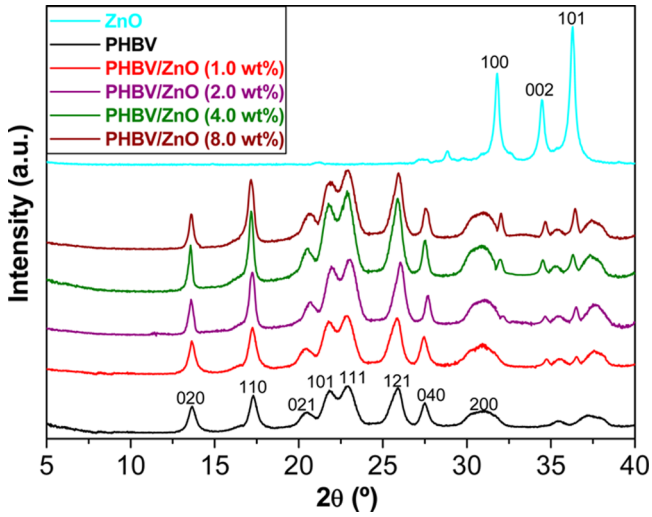

Figure 4. Room-temperature XRD patterns of PHBV, ZnO, and the nanocomposites.

neat PHBV shows main peaks at 2θ values of 13.6, 17.1, 20.3, 21.7, 22.8, 25.7, 27.4, and 30.8°, which correspond to the reflection of the (020), (110), (021), (101), (111), (121), (040), and (200) crystalline planes, respectively, of the orthorhombic unit cell that belongs to the space group $P2_12_12_1$ ($D2^4$).[38] These peaks are also observed in the patterns of the nanocomposites, together with those typical of the nanoparticles, indicating that the crystalline structure of both components is maintained. The nanocomposites display narrower and more intense peaks than the neat matrix, corroborating that ZnO nanoparticles act as nucleating agents for the matrix crystallization, leading to the formation of smaller and more perfect crystals, in agreement with DSC analysis. For instance, for the nanocomposite with 4.0 wt % ZnO, about 30% rise in the full width at half-maximum (fwhm) of the diffraction peak corresponding to the (110) plane is detected, pointing toward a reduction in the average crystallite size, since the peak width is inversely proportional to the crystallite size according to the Scherrer formula.[39] An analogous phenomenon has been previously reported for MWCNT-reinforced PHBV composites.[7] Nevertheless, the crystallite size of the nanocomposite with the highest loading is slightly bigger than that of the sample with 4.0 wt % ZnO, because the increased nanofiller−matrix interactions could impose a certain degree of confinement on the crystal growth.

Thermal Stability. One of the major shortcomings of PHBV is its low thermal stability, since thermal degradation can take place during the polymer melt processing. Consequently, it is important to investigate the effect of ZnO nanoparticles on the decomposition of this biopolymer. Figure 5 shows the TGA and DTG curves of ZnO, PHBV, and the nanocomposites under a nitrogen atmosphere, and their characteristic degradation temperatures, i.e., the initial degradation temperature at 2% weight loss (T_i), the temperature of 10% weight loss (T_{10}) and the temperature of maximum rate of degradation (T_{max}), are summarized in Table 1. The bare nanoparticles display a very small weight loss (~2.5 wt %) below 300 °C likely ascribed to the elimination of physically and chemically adsorbed water on their surface. Regarding neat PHBV, a single degradation stage can be observed that starts at ~298 °C and shows the maximum rate at around 350 °C (Table 1). The degradation occurs via chain scission mechanism, by a random

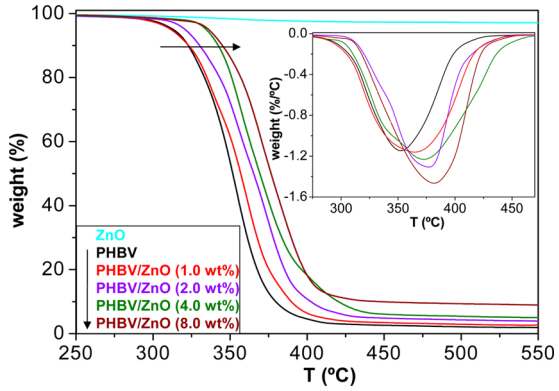

Figure 5. TGA curves under nitrogen atmosphere for neat PHBV, ZnO, and the nanocomposites with different nanoparticle loadings. The inset shows DTG curves of the polymeric samples.

cis-elimination reaction at a six-membered ring ester intermediate, producing unsaturated carboxyl acid and ester products.[40] A one-step decomposition process is also found for the nanocomposites, although shifted to higher temperatures, demonstrating the remarkable thermal stabilization effect induced by the presence of the nanoparticles. As shown in Table 1, T_{max} progressively rises upon increasing ZnO content, by up to 31 °C for the nanocomposite with 8.0 wt % loading. A similar trend is found for T_i and T_{10}, which show maximum increments of 22 and 25 °C, respectively. The good dispersion of ZnO within the matrix and the strong interactions between the two composite components via hydrogen bonding would originate a barrier effect against the transport of decomposition products from the bulk of the matrix to the gas phase. This effective barrier would hinder the formation of the six-membered ring ester groups, which combined with the high thermal conductivity of ZnO[41] that facilitates heat dissipation within the composite result in enhanced thermal stability for the nanocomposites. Moreover, a gradual raise in the char residue is observed with increasing ZnO content, indicating that a higher fraction of material did not volatilize upon thermal degradation. The nanoparticles act as insulator and mass transport barriers that obstruct the escape of volatile products generated during the degradation process and also prevent oxygen from reaching the matrix. It is worth noting that the increments in T_i and T_{max} obtained in this study are comparable to those found for CNC-reinforced PHBV nanocomposites[9] and higher than those reported upon incorporation of similar amounts of MWCNTs,[7] OMMT,[6] SiO_2,[33] or NFC.[34]

Tensile Properties. Inorganic nanofillers are frequently incorporated into biopolymers to improve the mechanical properties of the resulting composites. In particular, food packaging materials should have enough stiffness and strength to be self-supporting and resist handling damage. The room temperature static mechanical properties of PHBV/ZnO nanocomposites were evaluated by tensile tests, and representative stress–strain curves are shown in Figure 6a. Their values of Young's modulus (E), tensile strength (σ_y) and elongation at break (ε_b) are plotted as a function of ZnO concentration in Figure 6b–d. Neat PHBV has a Young's modulus of ~1.1 GPa, which rises gradually upon increasing nanoparticle concentration, showing a maximum increment of ~57% at 4.0 wt % ZnO, whereas it drops slightly at higher nanoparticle contents (Figure 6b). As known, the mechanical properties of polymer composites are influenced by many factors, including the state of dispersion of the filler, the degree of crystallinity of the matrix, and the filler–matrix interactions. Thus, the strong modulus improvement observed in these

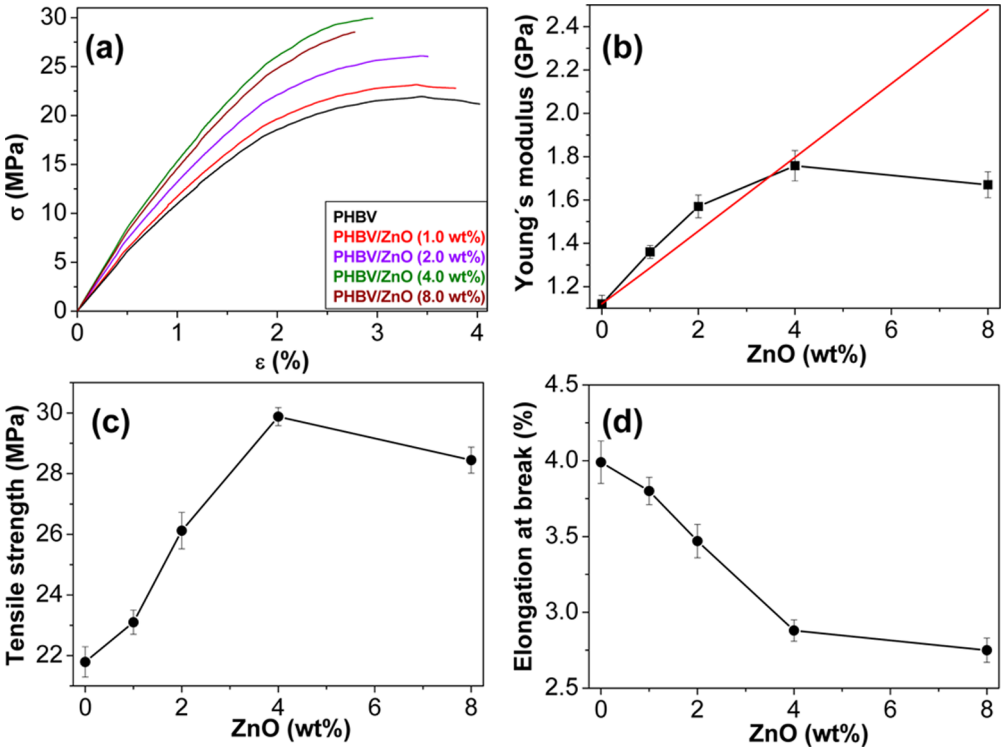

Figure 6. Tensile properties of neat PHBV/ZnO nanocomposites: (a) stress–strain curves; (b) Young's modulus; (c) tensile strength; (d) strain at break. The red straight line in Figure 4b corresponds to the theoretical predictions according to the Krenchel's rule of mixtures.

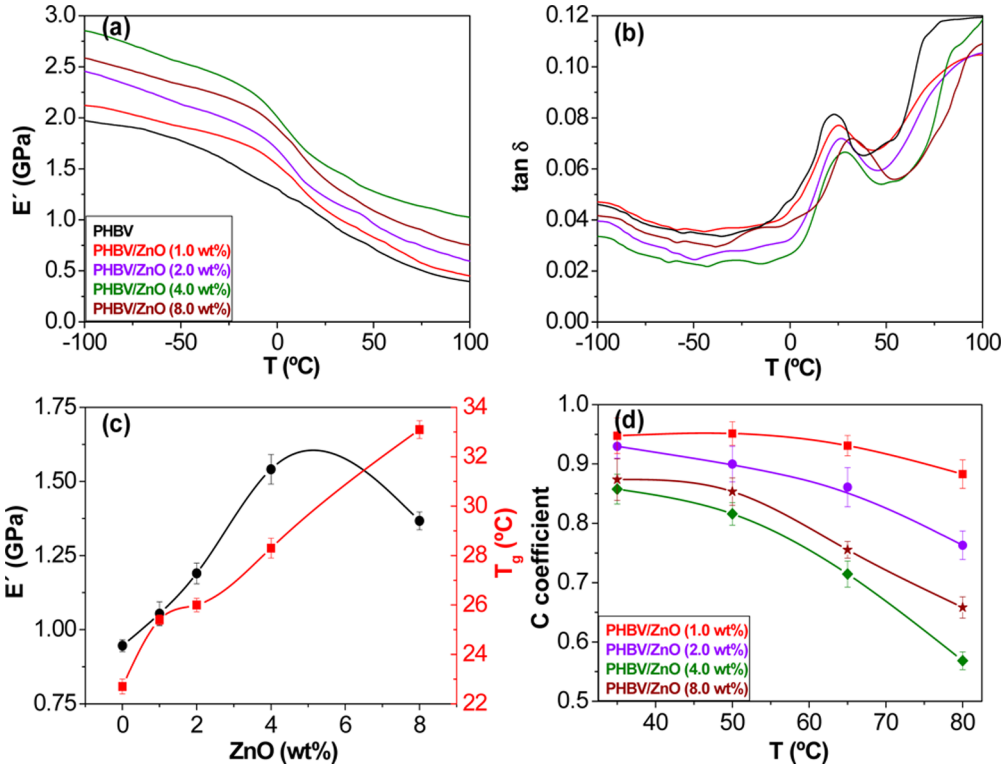

Figure 7. DMA measurements for PHBV/ZnO nanocomposites: (a) storage modulus E' and (b) tan δ as a function of temperature; (c) E' and T_g values as a function of ZnO content; (d) C coefficient at different temperatures.

bionanocomposites is likely ascribed to the combination of a very homogeneous nanoparticle dispersion, a strong interfacial adhesion between the phases through interactions via hydrogen bonding and the increase in the crystallinity of PHBV, as revealed by DSC analysis. However, at 8.0 wt % loading, small clusters composed of a few particles were detected, which reduce the matrix−nanoparticle interfacial contact area, and hence limit the stress transfer, as well as a small reduction in the level of crystallinity compared to the nanocomposite with 4.0 wt % ZnO, facts that could account for the smaller improvement in modulus. Regarding the tensile strength (Figure 6c), the trend observed is qualitatively similar to that described above for the modulus, albeit the increments in comparison to the value of neat PHBV are lower (about 32% increase at 4.0 wt % ZnO), suggesting that these nanoparticles are more effective in enhancing the stiffness than the strength of the biopolymer matrix. More importantly, their reinforcement effect is more effective than that reported for similar amounts of other nanofillers such as OMMT,[6] GO,[8] MWCNTs,[32] or NFC,[34] demonstrating that ZnO nanoparticles are highly suitable for enhancing the mechanical performance of biodegradable PHAs.

Considering the reported Young's modulus for ZnO,[42] the theoretical E values for the nanocomposites were estimated by the Krenchel's rule of mixtures for discontinuous reinforcement,[43] which can be written as $E_c = (\eta E_f - E_m)V_f + E_m$, where E_c, E_f, and E_m are the tensile modulus of the composite, filler, and matrix, respectively, V_f the filler volume fraction and η the strengthening coefficient that is assumed to be 1/5 for randomly oriented fillers. The results are plotted in Figure 6b as a red straight line. Theoretical Young's moduli of PHBV/ZnO nanocomposites are in good agreement with the experimental data (differences ≤7%), except for the nanocomposite with 8.0 wt %, where the measured value is about 33% lower than the calculated one. This discrepancy should be related to the fact that the model assumes perfect filler−matrix adhesion and optimal distribution of individual particles, whereas in the nanocomposite with the highest loading the nanofillers are not individually dispersed but forming small clusters. Therefore, it can be concluded that the ZnO nanoparticles are indeed individually dispersed and strongly adhered to the PHBV matrix at low filler concentrations.

On the other hand, the strain at break (Figure 6d) drops progressively with increasing ZnO content, by about 30% at the highest concentration tested. This is the typical behavior expected for filler-reinforced composites, because the fillers restrict the ductile flow of the polymer chains, which is reflected in lower ε_b values. Nevertheless, for similar nanofiller contents, the fall in tensile strain found for OMMT,[6] GO,[8] CNC,[9] or MWCNT-reinforced PHBV[32] is stronger (i.e., about 50% at 3.0 wt % MWCNT), likely related to poorer nanofiller dispersion. The hydrogen bonding interactions between ZnO and the biopolymer prevent nanoparticle aggregation, resulting in fewer stress concentration sites, and thus minimizing the reduction in ductility.

Dynamic Mechanical Analysis. Packaging materials are commercially used below room temperature (i.e., at frozen food storage temperatures from −30 to −18 °C or refrigeration conditions between 3 and 6 °C), hence it is important to assess their mechanical performance under such conditions. The temperature dependence of the storage modulus (E′) and loss factor (tan δ) for neat PHBV and the composites with different ZnO contents was investigated by DMA, and representative curves are displayed in panels a and b in Figure 7, respectively. E' values at 25 °C as a function of ZnO loading are plotted in Figure 7c. Semicrystalline PHBV exhibits a continuous but

gentle decline in modulus with increasing temperature, less pronounced than that reported for other biopolymers like poly(lactide acid) (PLA), in agreement with the results reported previously.[44] At temperatures below the glass transition (T_g), a significant improvement in E' is found upon increasing ZnO concentration, which confirms the remarkable reinforcing effect of these nanoparticles. In fact, the storage modulus reveals the capability of a material to store mechanical energy without dissipation; the higher the storage modulus, the stiffer the material is. Thus, at −100 °C, a maximum modulus increment of ∼44% is attained for the nanocomposite with 4.0 wt % ZnO. This improvement should also be related to the increase in the crystallinity of the matrix, since the crystalline regions enhance the modulus of semicrystalline polymers, along with a strong filler−matrix interfacial adhesion due to hydrogen bonding interactions between the −OH groups of ZnO and the C═O and −O− groups of PHBV, as mentioned previously. Nevertheless, the enhancement in modulus is larger at temperatures above T_g (i.e., about 150% increase at 100 °C for the nanocomposite with 4.0 wt % loading compared to that of neat PHBV). This indicates that the stiffening effect is more pronounced above the softening point of the matrix, in agreement with the results reported for NFC-reinforced PHBV nanocomposites.[34] This behavior has been attributed to the formation of a percolated system of nanofiller held together by hydrogen bonding at higher temperatures.

As can be observed in Figure 7c, the storage modulus grows almost linearly with increasing ZnO loading, showing a maximum at 4.0 wt % (around 60% increase compared to the neat biopolymer), whereas it decreases slightly for the nanocomposite with 8.0 wt % ZnO, consistent with the results from tensile tests. The effectiveness of fillers on the moduli of composites can be described by a coefficient C determined by the equation:[44] $C = (E'_g/E'_r)_{comp}/(E'_g/E'_r)_{polym}$, where E'_g and E'_r are the storage modulus values in the glassy and rubbery regions, respectively. This coefficient represents the ability to disturb the motion of polymer chains, and depends on a large number of factors including the polymer nature, the filler concentration, and size distribution, as well as the filler−filler and filler−matrix interactions. Basically, the lower the C coefficient, the higher the effectiveness of the reinforcement. The coefficient was calculated at four temperatures (35, 50, 65, and 80 °C), taking E'_g at −50 °C, and the results are plotted in Figure 7d. For all the nanocomposites, C decreases with increasing temperature, indicating better reinforcement effect at elevated temperatures, as inferred from Figure 7a. Under such conditions, the polymer loses the elastic response and the viscous behavior begins to dominate. Therefore, E' of the polymer decreases, while the stiffness of the nanoparticles remains unchanged because they do not undergo any thermally induced transition, increasing their effectiveness on the composite modulus. On the other hand, the minimum C values are found for the nanocomposite with 4.0 wt % ZnO, confirming that this is the optimal nanoparticle loading for improving the polymer mechanical performance.

The damping factor (tan δ, ratio of the loss to storage modulus) gives information about the energy lost in a system due to deformation, and is related to the impact resistance of a material. As depicted in Figure 7b, the plot of tan δ as a function of temperature for PHBV shows an intense maximum named α relaxation that corresponds to the T_g at about 23 °C. The low temperature relaxation (γ) at around −100 °C, related to the presence of absorbed water in the amorphous domains, as well as the α_c relaxation in the range of 80−130 °C attributed to motions of the crystalline phase can only be inferred in the DMA spectrum of this biopolymer.[45] With regard to T_g data for the different nanocomposites (Figure 7c), it is found that the addition of ZnO leads to a shift of this transition temperature toward higher values; this suggests restrained mobility of the polymer chains in the presence of the quasi-spherical nanoparticles. In particular, T_g increases by ∼10 °C for the nanocomposite with the highest ZnO content in comparison to that of pure PHBV. Given that the glass transition is associated with the mobility of chain segments in the amorphous regions, a reasonable explanation is that those segments in the vicinity of the nanoparticles are less mobile, because these hamper rotational motion within the chains, and therefore lead to an increase in T_g. An analogous behavior of T_g increment has been reported for PHBV composites reinforced with NFC, though the increases were smaller.[34]

It can also be observed from Figure 7b that the maximum value of tan δ is lower for the nanocomposites compared to that of the neat matrix. The magnitude of the tan peak δ is indicative of the nature of the polymer system. In an unfilled system, the chain segments are free from restraints. The introduction of the nanoparticles causes a reduction in chain mobility, thus reducing the peak height. Moreover, a high value of tan δ typically implies imperfections in the elasticity of a system. Therefore, the lower tan δ in the nanocomposites suggests that when the stress is removed, the energy stored in deforming the material is recovered more quickly compared to the unfilled polymer. Additionally, a remarkable broadening of tan δ is found on increasing nanoparticle content. In particular, the peak width at half height increases from 15 °C for neat PHBV to 24 °C for the nanocomposite with 8.0 wt % ZnO. This effect could arise from a more heterogeneous amorphous phase in the nanocomposites compared to that of the neat matrix, and has also been interpreted as larger volume of the interface.[44] Thus, a rise in the nanoparticle content would result in increased nanoparticle−matrix interactions via hydrogen bonding and larger interfacial area, and the molecular motions at the interface region also contribute to the damping of the material.[45] Overall, DMA results demonstrate that the developed nanocomposites display good rigidity under normal freezing and refrigeration conditions, showing considerably improved performance compared to mthat of the neat biopolymer.

Impact Strength. Neat PHBV presents several shortcomings for commercial use as food packaging material, including a high crystallinity of about 55%, which causes an inherent brittleness and poor impact resistance. Consequently, it is of great importance to enhance the impact strength of this biopolymer via addition of nanofillers. The results from Charpy notched impact strength measurements of PHBV and its nanocomposites are depicted in Figure 8. The incorporation of low nanoparticle loadings results in a noticeable improvement in the impact resistance of PHBV, by ∼28% for the nanocomposite with 2.0 wt % ZnO, consistent with the increase in the area under the tensile curve, which is a measure of the toughness of the material. A small enhancement is also observed for the composite with 4.0 wt % ZnO, whereas that with 8.0 wt % loading exhibits approximately the same impact strength as the neat thermoplastic. This dependence of the impact strength on the ZnO content was already anticipated from the analysis of the area under tan δ peaks (Figure 7b),

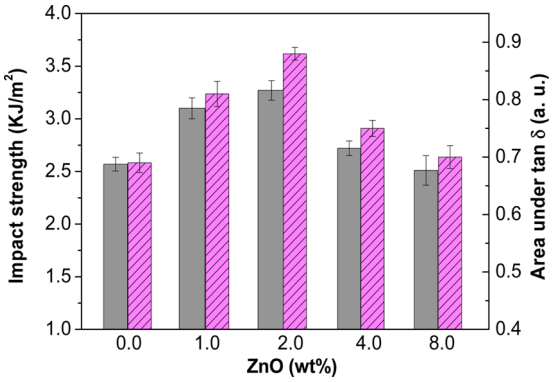

Figure 8. Comparison of the Charpy notched impact strength (solid bars) and the area under tan δ curve (dashed bars) for PHBV and its nanocomposites.

since it is representative of the energy dissipated in viscoelastic relaxations, hence it is indicative of the toughness of the material. In fact, any molecular process that promotes energy dissipation enhances the impact resistance of the polymer. As can be observed in Figure 8, all the nanocomposites display larger area than the neat polyester except that with the highest loading that exhibits roughly the same value. The results obtained by the two techniques display qualitatively similar trend, and demonstrate that the incorporation of small amounts of these nanoparticles improve the ability of PHBV to absorb energy during the deformation process.

It is well-known[46] that the shape, size, state of dispersion of the filler, and its interfacial adhesion with the matrix have strong influence on the rate of energy absorption, hence on the impact properties of polymer composites. The toughness of PHBV improves significantly upon incorporation of low ZnO contents, attributed to a very homogeneous nanofiller dispersion that minimizes the stress concentration nuclei, as well as an enhanced interfacial adhesion between the composite phases via hydrogen bonding that would provide an effective barrier for pinning and bifurcation of the advancing cracks. Nevertheless, in the sample with the highest ZnO loading, the presence of small clusters might nucleate a few cracks and/or reduce the nanofiller−matrix interfacial area. Overall, the impact resistance of the polymer is approximately maintained in this nanocomposite.

Antibacterial Properties. The addition of antimicrobial compounds to food packaging materials has recently received considerable attention.[3] Nanocomposite antimicrobial systems are particularly effective because of the high surface to volume ratio and enhanced surface reactivity of the nanosized antimicrobial agents, making them able to restrict the growth of pathogenic and spoilage microorganisms more effectively than their micro- or macroscale counterparts. Metal nanoparticles (Ag, Cu, Au), metal oxide nanomaterials (TiO_2, ZnO, MgO), and carbon nanotubes are the most frequently employed nanofillers to develop antimicrobial action. Albeit Ag has been traditionally used as an antimicrobial agent in food and beverage storage applications, ZnO nanoparticles are expected to provide a more affordable and safe food packaging solution in the future. In this regard, the antibacterial action of PHBV nanocomposites was evaluated against two human pathogen bacteria: *E. coli* (Gram-negative) and *S. aureus* (Gram-positive), and the results are shown in Figure 9a. To better assess the influence of the nanofiller content, we also tested nanocomposites with 5.0 and 5.5 wt % ZnO. Clearly, the

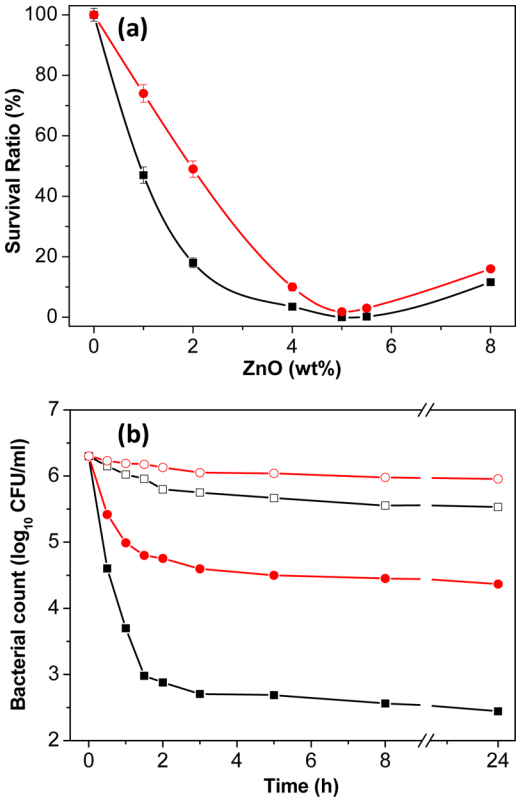

Figure 9. (a) Effect of PHBV/ZnO nanocomposites on the survival ratio of *E. coli* (black squares) and *S. aureus* (red circles). (b) Kinetics of the antibacterial activity of PHBV/ZnO nanocomposites with 2.0 and 5.0 wt % loading (open and solid symbols, respectively) against *E. coli* (squares) and *S. aureus* (circles).

survival ratio of both bacteria drops sharply upon increasing ZnO concentration, and the best antibacterial activity is found for the nanocomposite with 5.0 wt % loading. This notable bacterial inactivation could be explained in terms of the very homogeneous nanoparticle dispersion in the composites, hence large antimicrobial surface. Nevertheless, the nanocomposite with 8.0 wt % loading displays reduced bactericide effect in comparison to those with ZnO content in the range of 4.0−5.5 wt %, which should be related to its poorer nanoparticle dispersion, as discussed earlier. Indeed, the efficiency of the antibacterial function of polymer nanocomposites is greatly influenced by various factors such as particle size, distribution and interaction with the polymer matrix.[3] In order to fully exploit the antimicrobial properties of nanoparticles, they should be homogeneously dispersed without the formation of aggregates. Further, the antibacterial activity has been found to improve with decreasing particle size.[47] Thus, the small clusters in the composite with 8.0 wt % ZnO could behave as larger particles, thereby exhibiting less antimicrobial activity than the individual nanoparticles.

To obtain information about the kinetics of the antibacterial activity, residual colony-forming units (CFUs) were counted at different time intervals, and the data for nanocomposites with 2.0 and 5.0 wt % ZnO are shown in Figure 9b. Most significantly, the sample with 5.0 wt % nanoparticle content displays strong and rapid bactericidal action against *E. coli*, resulting in almost 4-log reduction in 3 h. In contrast, for the same bacteria, the nanocomposite with 2.0 wt % shows slower biocide effect, causing less than 1-log drop, which confirms the

dx.doi.org/10.1021/am502261e | ACS Appl. Mater. Interfaces 2014, 6, 9822−9834

strong dependence of the bactericide activity on the ZnO concentration. Analogous trend is found against *S. aureus*, albeit with smaller reductions in the number of CFUs.

On the other hand, Figure 9a and b reveal that the antibacterial effect of PHBV nanocomposites on *E. coli* is systematically stronger than on *S. aureus*, consistent with previous studies[48] that reported more effective action of ZnO nanoparticles against Gram-negative bacteria. The different behavior against the two types of bacteria has been ascribed to structural and chemical compositional differences of the cell surfaces.[49] Thus, Gram-positive bacteria usually have one cytoplasmic membrane and a thick wall composed of multilayers of peptidoglycan, whereas the Gram-negative have a more complex cell wall structure, with a layer of peptidoglycan between the outer membrane and the cytoplasmic membrane.

Several mechanisms have been proposed to explain the antibacterial activity of ZnO nanoparticles:[49,50] the mechanical damage of the cell membranes caused by penetration of the nanofillers, the release of Zn^{2+} ions, and the production of H_2O_2 from the nanoparticle surface. Tam et al.[47] analyzed numerous bacteria cells exposed to ZnO (~10 nm diameter) and found very few cases of nanoparticle internalization. In the current study, the nanoparticles possess a mean diameter of 75 nm, thus are not likely to penetrate into the cell wall to damage the bacteria from the interior. On the other hand, ZnO is in general unstable in solution even without illumination,[47] and the Zn^{2+} concentration increases as a result of ZnO decomposition; therefore, the release of Zn^{2+} is a potential reason for the biocide action. These nanocomposites exhibit antimicrobial action in the absence of UV light, which is consistent with the studies by Yamamoto et al.[51] and Tam et al.[47] who demonstrated that the antibacterial activity of ZnO nanomaterials without irradiation was associated with the release of H_2O_2 from the ZnO surface. The process seems to be related to the moisture absorption by the material that facilitates H_2O_2 production,[52] albeit the exact mechanism of action remains still unclear. Thus, the generation of H_2O_2 (a strong oxidizing agent detrimental to the cells of living organisms) could be regarded as the main factor of antibacterial activity of these nanocomposites, and the different action against *E. coli* and *S. aureus* likely originates from the different sensitivities toward the H_2O_2 produced. Overall, results demonstrate the potential of the developed nanocomposites to prevent microbial proliferation occurring in packaged food during storage.

Barrier and Migration Properties. One of the main goals when adding nanofillers to polymers used for food packages is to improve their barrier properties to gases, vapors and organic compounds. Excess moisture and oxygen are leading causes of food spoilage, and thus these are the two main permeants studied in packaging applications, because they may transfer from the internal or external environment through the composite package wall, resulting in a continuous change in product quality and shelf life.[1] Nevertheless, the specific barrier requirements depend on the product characteristics and the intended end-use application. For example, materials used for carbonated beverage containers should have a high oxygen barrier in order to prevent oxidation of the beverage contents, whereas in packages for fresh fruits and vegetables, high barriers to oxygen diffusion are undesirable.[1]

In this study, the water vapor permeability (WVP, amount of water vapor that permeates per unit of area and time in a packaging material) and the water uptake of the nanocomposites were tested, and the results are plotted in Figure 10a. As can be observed, both parameters drop gradually with

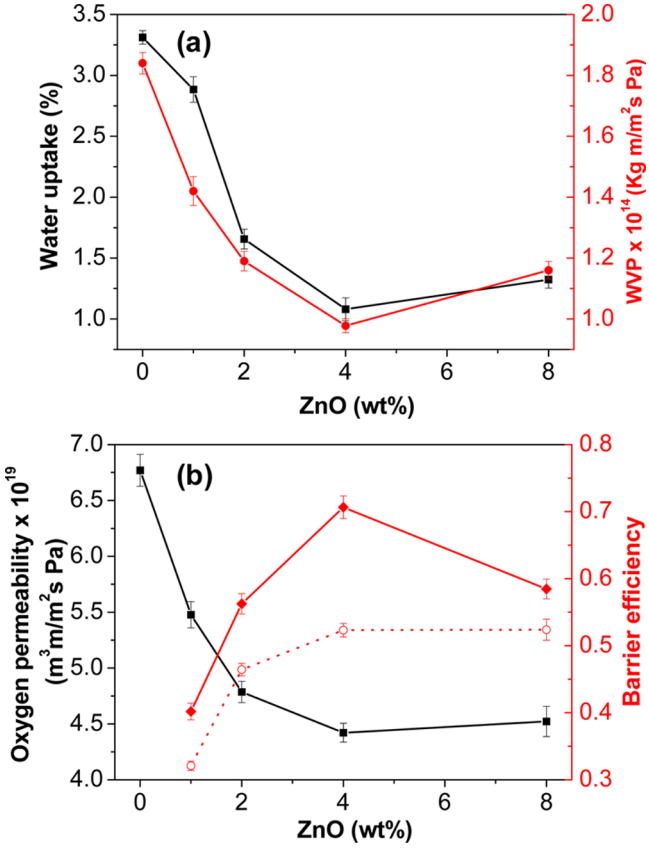

Figure 10. Barrier properties of PHBV/ZnO nanocomposites as a function of ZnO content: (a) water uptake and water vapor permeability (WVP); (b) oxygen permeability and barrier efficiency for water (solid diamonds) and oxygen (open circles).

increasing ZnO concentration, showing a minimum value (about 46 and 69% decrease, respectively) at a critical nanofiller loading of 4.0 wt %, which reveals improved barrier properties against water and water vapor for the nanocomposites in comparison to the neat biopolymer. These improvements are larger than those reported for MWCNT[7] or carbon nanofiber-reinforced PHBV,[53] and comparable to those found for composites incorporating nanoclays.[54] The behavior found in PHBV/ZnO nanocomposites likely arises from a competition of water affinity, degree of crystallinity, and tortuosity effects. On the one hand, ZnO is more hydrophilic than PHBV, hence the hydrophilicity of the nanocomposites should increase with the nanoparticle content. On the other hand, the crystallinity rises with the ZnO loading, as revealed by DSC analysis, reaching a maximum value at 4.0 wt %, and water molecules are unable to permeate the polymer crystallites because they are insoluble in the material. In addition, the increase in both ZnO loading and crystallinity leads to higher tortuosity of the transport path.[53] It appears that the increase in crystallinity and level of tortuosity outweigh the raise in hydrophilicity, and the overall result is a diminution in the water uptake and WVP. In the case of the nanocomposite with the highest loading, the reduction in both parameters is smaller than that of the sample with 4.0 wt %, probably because of the lower crystallinity and the presence of small nanoparticle clusters which might result

dx.doi.org/10.1021/am502261e | ACS Appl. Mater. Interfaces 2014, 6, 9822−9834

in preferential penetrant pathways that have detrimental effects on the barrier performance.

Focusing on the oxygen permeability of the nanocomposites (Figure 10b), a noticeable reduction is also observed as the ZnO content rises, by up to 35% for the nanocomposite with 4.0 wt % loading in comparison to the value of neat PHBV, hence demonstrating the blocking capacity of the highly crystalline ZnO. This enhanced barrier performance should be related to the very homogeneous ZnO dispersion, its strong interfacial adhesion with the polyester matrix that causes chain immobilization, hence decreased diffusion, combined with the increase in the degree of crystallinity of the matrix. However, raising the nanoparticle content to 8.0 wt % does not result in further oxygen barrier improvement, despite the increased ZnO-matrix interactions, probably because filler clustering initiates, which could lead to the formation of preferential paths for the permeants to diffuse faster. An analogous behavior has been reported for PHBV nanocomposites filled with nanoclay,[54] where the oxygen permeability decreased significantly up to 5.0 wt % nanofiller loading and then remained merely unchanged. Overall, results indicate that the barrier performance is the consequence of a balance between polymer structural morphology (i.e., crystalline phase content), nanoparticle dispersion, and loading.

To obtain more information about the barrier properties, we determined the clay barrier efficiency for each nanocomposite and permeant (water and oxygen) (Figure 10b). This factor was calculated by dividing the permeability drop in percent between the sample degree of crystallinity as determined by DSC, and indicates the barrier effect of the nanofiller independently of the composite crystallinity. The results corroborate that 4.0 wt % is the most effective nanoparticle loading, particularly against water permeation, and that the nanoparticles reinforce more efficiently against water than against oxygen.

Migration is the quantity of packaging material, principally additives, which can be transferred to foodstuff. Generally, migration has been regarded as a negative issue because many substances represent a danger to human health and/or modify the food composition. Overall migration tests with nonpolar and polar simulants were conducted to determine the total amount of nonvolatile substances that might migrate into foodstuff from PHBV and its nanocomposites. The results from experiments performed in isooctane and 10% (v/v) ethanol are displayed in Figure 11. It is important to highlight that, for both simulants, the maximum migration levels are well below the migration limits (60 mg/kg or 10 mg/dm^2 of simulant) for food contact materials established by current legislation (commission directive, 2002/72/EC).[55] More importantly, increasing the ZnO content strongly reduces the migration in ethanol 10% (v/v), by up 59% at 4.0 wt % loading, which should be related to the improved nanoparticle dispersion and strong adhesion with the matrix chains, as discussed previously. A decreasing trend is also found for migration in isooctane, the maximum fall being ~34% at the same critical ZnO concentration. In this case, the migration levels are lower compared to those in ethanol, consistent with the results reported for other composites based on polyester matrices such as PLA.[55] The different migration values found for both simulants probably arise from solubility and polarity differences between the polymer, nanofiller, migrants and the food simulant, since such thermodynamic properties play a key role on the overall migration. Regarding the nanocomposite with the highest loading, both migration levels were slightly higher than those of the sample with 4.0 wt %, likely due to the poorer nanoparticle dispersion that causes a reduction in matrix homogeneity and cohesion, which has a negative effect on the migration properties. On the whole, results demonstrate that the incorporation of ZnO to PHBV has a positive effect on both barrier and migration properties, rendering improved biodegradable materials that show great potential as containers for oxygen- and/or moisture-sensitive food products.

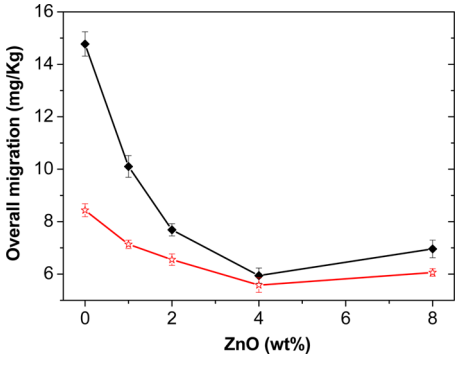

Figure 11. Overall migration data in ethanol 10% (v/v) (solid diamonds) and isooctane (open stars) for PHBV and its bionanocomposites.

4. CONCLUSIONS

Biodegradable PHBV-based nanocomposites reinforced with uniformly dispersed ZnO nanoparticles were successfully prepared via simple solution casting method without the need for surfactants or coupling agents. Their morphology, thermal, mechanical, barrier, migration and antibacterial properties were investigated. The nanoparticles acted as nucleating agents, increasing the crystallization temperature and the level of crystallinity of PHBV while decreasing its crystallite size. Moreover, they strongly enhanced its thermal stability, attributed to their barrier effect that delayed the transport of decomposition products from the bulk of the composite to the gas phase. A remarkable increase in both the storage modulus and glass transition temperature of the matrix was found upon addition of ZnO, the stiffening effect being more pronounced at temperatures above the glass transition. The tensile and barrier properties of the biopolymer were also noticeably enhanced, ascribed to the very homogeneous nanofiller dispersion, its strong interfacial adhesion with PHBV combined with the increase in the crystallinity of the matrix. The nanocomposites exhibited antibacterial activity against human pathogenic bacteria, and the effect on *E. coli* was systematically stronger than on *S. aureus*. Further, their overall migration levels in both nonpolar and polar simulants decreased with increasing nanoparticle content, and were well below the current legislative limits for food packaging materials. At a critical concentration of 4.0 wt % ZnO, which leads to an optimal balance between structural morphology (highest crystallinity), nanoparticle state of dispersion (random and homogeneous) and number of hydrogen bonding interactions between the −OH groups of the ZnO surface and the polar moieties of the biopolymer, the tensile strength, Young's and storage moduli showed a maximum that coincided with the minimum water uptake, water vapor permeability, oxygen permeability and migration levels. These sustainable bionano-

composites with antimicrobial function show great potential as an alternative to synthetic plastic packaging materials, since they can restrict the growth of pathogenic and spoilage microorganisms, hence extending shelf life and preserving the quality and safety of food products during transportation and storage. In particular, they are very promising to be used as packaging materials for cheese, cereals, bakery, and meat products as well as for the manufacture of thermoformed containers for fruit juices and dairy products, or bottles for water, beer, or carbonated drinks. They can also be suitable for disposable applications like disposable cutlery, cups and utensils, blister packages, trash bags, overwrap, and lamination films.

AUTHOR INFORMATION

Corresponding Author

*E-mail: adiez@ictp.csic.es.

Notes

The authors declare no competing financial interest.

ACKNOWLEDGMENTS

A.M.D.-P. acknowledges the Consejo Superior de Investigaciones Científicas (CSIC) for a JAE Postdoctoral Fellowship cofinanced by the EU.

REFERENCES

(1) Siracusa, V.; Rocculi, P.; Romani, S.; Rosa, M. D. Biodegradable Polymers for Food Packaging: a Review. *Trends Food Sci. Technol.* **2008**, *19*, 634−643.

(2) Rhim, J.-W.; Park, H.-M.; Ha, C.-S. Bio-nanocomposites for Food Packaging Applications. *Prog. Polym. Sci.* **2013**, *38*, 1629−1652.

(3) Laycock, B.; Halley, P.; Pratt, S.; Werker, A.; Lant, P. The Chemomechanical Properties of Microbial Polyhydroxyalkanoates. *Prog. Polym. Sci.* **2013**, *38*, 536−583.

(4) Shah, A.; Hasan, F.; Hameed, A.; Ahmed, S. Niological Degradation of Plastics: a Comprehensive Review. *Biotechnol. Adv.* **2008**, *26*, 246−265.

(5) Cheng, L.; Wang, M. Production and Evaluation of Biodegradable Composites Based on PHB-PHV Copolymer. *Biomaterials* **2002**, *23*, 2631−2639.

(6) Hema, R.; Ng, P. N.; Amirul, A. A. Green Nanobiocomposite: Reinforcement Effect of Montmorillonite Clays on Physical and Biological Advancement of Various Polyhydroxyalkanoates. *Polym. Bull.* **2013**, *70*, 755−771.

(7) Yu, H.-Y.; Qin, Z.-Y.; Sun, B.; Yang, X.-G.; Yao, J.-M. Reinforcement of Transparent Poly(3-hydroxybutyrate-co-3-hydroxyvalerate) by Incorporation of Functionalized Carbon Nanotubes as a Novel Bionanocomposite for Food Packaging. *Compos. Sci. Technol.* **2014**, *94*, 96−104.

(8) Sridhar, V.; Lee, I.; Chun, H. H.; Park, H. Graphene Reinforced Biodegradable Poly(3-hydroxybutyrate-*co*-4-hydroxybutyrate) Nanocomposites. *Express Polym. Lett.* **2013**, *7*, 320−328.

(9) Yu, H.-Y.; Qin, Z.-Y.; Liu, Y.-N.; Chen, L.; Liu, N.; Zhou, Z. Simultaneous Improvement of Mechanical Properties and Thermal Stability of Bacterial Polyester by Cellulose Nanocrystals. *Carbohydr. Polym.* **2012**, *89*, 971−978.

(10) Jiang, L.; Morelius, E.; Zhang, J.; Wolcott, M.; Holbery, J. Study of the Poly(3-hydroxybutyrate-co-3-hydroxyvalerate)/Cellulose Nanowhisker Composites Prepared by Solution Casting and Melt Processing. *J. Compos. Mater.* **2008**, *42*, 2629−2645.

(11) Curridal, M. L.; Comparelli, R.; Cozzli, P. D.; Mascolo, G.; Agostiano, A. Colloidal Oxide Nanoparticles for the Photocatalytic Degradation of Organic Dye. *Mater. Sci. Eng., C* **2003**, *23*, 285−289.

(12) Lin, H. M.; Tzeng, S. J.; Hsiau, P. J.; Tsai, W. L. Electrode Effects on Gas Sensing Properties of Nanocrystalline Zinc Oxide. *Nanostruct. Mater.* **1998**, *10*, 465−477.

(13) Oh, J.-Y.; Lim, S.-C.; Ahn, S. D.; Lee, S. S.; Cho, K.-I.; Koo, J. B.; Choi, R.; Hasan, M. Facile One-step Synthesis of Magnesium-doped ZnO nanoparticles: Optical Properties and Their Device Applications. *J. Phys. D: Appl. Phys.* **2013**, *46*, 285101−285107.

(14) Zhang, L.; Jiang, Y.; Ding, Y.; Povey, M.; York, D. Investigation into the Antibacterial Behavior of Suspensions of ZnO Nanoparticles (ZnO Nanofluids). *J. Nanopart. Res.* **2007**, *9*, 479−489.

(15) Diez-Pascual, A. M.; Diez-Vicente, A. L. Development of Nanocomposites Reinforced with Carboxylated Poly(ether ether ketone)-grafted to Zinc Oxide with Superior Antibacterial Properties. *ACS Appl. Mater. Interfaces* **2014**, *6*, 3729−3741.

(16) Diez-Pascual, A. M.; Xu, C. P.; Luque, R. Development and Characterization of Novel Poly(ether ether ketone)/ZnO Bionanocomposites. *J. Mater. Chem. B* **2014**, *2*, 3065−3078.

(17) Ma, X.-Y.; Zhang, W.-D. Effects of Flower-like ZnO Nanowhiskers on the Mechanical, Thermal and Antibacterial Properties of Waterborne Polyurethane. *Polym. Degrad. Stab.* **2009**, *94*, 1103−1109.

(18) Chang, B. P.; Akil, H. M.; Nasir, R. M.; Nurdijati, S. Abrasive Wear Performance and Antibacterial Assessment of Untreated and Treated ZnO-reinforced Polymer Composite. *Polym. Compos.* **2013**, *34*, 1020−1032.

(19) Li, F.; Hu, L.; Li, Z.; Huang, X. Influence of Temperature on the Morphology and Luminescence of ZnO Micro and Nanostructures Prepared by CTAB-assisted Hydrothermal Method. *J. Alloys Compd.* **2008**, *465*, L14−L19.

(20) Rataboul, F.; Nayral, C.; Casanove, M. J.; Maisonnat, A.; Chaudret, B. Synthesis and Characterization of Monodisperse Zinc and Zinc Oxide Nanoparticles from the Organometallic Precursor [Zn(C6H11)2]. *J. Organomet. Chem.* **2002**, *643*−*644*, 307−312.

(21) Suwanboon, S.; Amornpitoksuk, P.; Haidoux, A.; Tedenac, J. C. Structural and Optical Properties of Undoped and Aluminium Doped Zinc Oxide Nanoparticles via Precipitation Method at Low Temperature. *J. Alloys Compd.* **2008**, *462*, 335−339.

(22) Yamada, H.; Suzuki, K.; Koizumi, S. Gene Expression Profile in Human Cells Exposed to Zinc. *J. Toxicol. Sci.* **2007**, *32*, 193−196.

(23) Jin, T.; Sun, D.; Su, J. Y.; Zhang, H.; Sue, H. J. Antimicrobial Efficacy of Zinc Oxide Quantum Dots Against Listeria Monocytogenes, Salmonella Enteritidis, and Escherichia Coli O157:H7. *J. Food Sci.* **2009**, *74*, 46−52.

(24) Emamifar, A.; Kadivar, M.; Shahedi, M.; Solaimanian-Zad, S. Evaluation of Nanocomposite Packaging containing Ag and ZnO on the Shelf Life of Fresh Orange Juice. *Innov. Food Sci. Emerg. Technol.* **2010**, *11*, 742−748.

(25) Yu, W.; Lan, C.-H.; Wang, S.-J.; Fang, P.-F.; Sun, Y.-M. Influence of Zinc Oxide Nanoparticles on the Crystallization Behaviour of Electrospun Poly(3-hydroxybutyrate-co-3-hydroxyvalerate) Nanofibers. *Polymer* **2010**, *51*, 2403−2409.

(26) Buzarovska, A.; Bogoeva-Gaceva, G.; Grozdanov, A.; Avella, M.; Gentile, G.; Errico, M. Crystallization Behavior of Poly-(hydroxybutyrate-co-valerate) in Model and Bulk PHBV/Kenaf Fiber Composites. *J. Mater. Sci.* **2007**, *42*, 6501−6509.

(27) ASTM D 638-03, Standard Test Method for Tensile Properties of Plastics. In *Annual Book of ASTM*; ASTM: Philadelphia, PA, 2003; pp 162−170.

(28) ASTM D 6110-10, Standard Test Method for Determining the Charpy Impact Resistance of Notched Specimens of Plastics. In *Annual Book of ASTM*; ASTM: Philadelphia, PA, 2010.

(29) ASTM E96-95, Standard Test Methods for Water Vapor Transmission of Materials. In *Annual Book of ASTM*; ASTM: Philadelphia, PA, 1995; pp 406−413.

(30) ASTM D3985-05, Standard Test Method for Oxygen Gas Transmission Rate Through Plastic Film and Sheeting Using a Coulometric Sensor. In *Annual Book of ASTM*; ASTM: Philadelphia, PA, 2010.

(31) EN-1186-1, Materials and Articles in Contact with Foodstuffs. In *Plastics: Part 1. Guide to the Selection of Conditions and Test Methods for Overall Migration*; CEN, European Committee for Standardization: Brussels, Belgium, 2002.

(32) Vidhate, S.; Innocentini-Mei, L.; D'Souza, N. A. Mechanical and Electrical Multifunctional Poly(3-hydroxybutyrate-co-3-hydroxyvalerate)-Multiwall Carbon Nanotube Nanocomposites. *Polym. Eng. Sci.* **2012**, *52*, 367−1374.
(33) Ma, P. M.; Wang, R. Y.; Wang, S. F.; Zhang, Y.; Zhang, Y. X.; Hristova, D. Effects of Fumed Silica on the Crystallization Behavior and Thermal Properties of Poly(hydroxybutyrate-co-hydroxyvalerate). *J. Appl. Polym. Sci.* **2008**, *108*, 1770−1777.
(34) Srithep, Y.; Ellingham, T.; Peng, J.; Sabo, R.; Clemons, C.; Turng, L.-S.; Pilla, S. Melt Compounding of Poly(3-hydroxybutyrate-co-3-hydroxyvalerate)/Nanofibrillated Cellulose Nanocomposites. *Polym. Degrad. Stab.* **2013**, *98*, 1439−1449.
(35) Owen, A. J.; Heinzel, J. Crystallization and Melting Behaviour of PHB and PHB/HV Copolymer. *Polymer* **1992**, *33*, 1563−1567.
(36) Gunaratne, L. M. W. K.; Shanks, R. A.; Amarasinghe, G. Thermal History Effects on Crystallisation and Melting of Poly(3-hydroxybutyrate). *Thermochim. Acta* **2004**, *423*, 127−135.
(37) Liu, W. J.; Yang, H. L.; Wang, Z.; Dong, L. S.; Liu, J. J. Effect of Nucleating Agents on the Crystallization of Poly(3-hydroxybutyrate-co-3-hydroxyvalerate). *J. Appl. Polym. Sci.* **2002**, *86*, 2145−2152.
(38) Scandola, M.; Ceccorulli, G.; Pizzoli, M.; Gazzano, M. Study of the Crystal Phase and Crystallization Rate of Bacterial Poly(3-hydroxybutyrate-co-3-hydroxyvalerate). *Macromolecules* **1992**, *25*, 1405−1410.
(39) Alexander, L. E.; Krieger, R. E. *X-ray Diffraction Methods in Polymer Science*; Wiley: New York, 1969.
(40) Cheng, M. L.; Sun, Y. M.; Chen, H.; Jean, Y. C. Change of Structure and Free Volume Properties of Semi-crystalline Poly(3-hydroxybutyrate-co-3- hydroxyvalerate) During Thermal Treatments by Positron Annihilation Lifetime. *Polymer* **2009**, *50*, 1957−1964.
(41) Huang, Z. X.; Tang, Z. A.; Yu, J.; Bai, S. Thermal Conductivity of Nanoscale Polycrystalline ZnO Thin Films. *Physica B* **2011**, *406*, 811−823.
(42) Kucheyev, S. O.; Bradby, J. E.; Williams, J. S.; Jagadish, C.; Swain, M. V. Mechanical Deformation of Single-Crystal ZnO. *Appl. Phys. Lett.* **2002**, *80*, 956−958.
(43) Krenchel, H. *Fibre Reinforcement*; Akademisk Forlag: Copenhagen, Denmark, 1964.
(44) Adam, J.; Korneliusz, B. A.; Agnieszka, M. Dynamic Mechanical Thermal Analysis of Biocomposites Based on PLA and PHBV-a Comparative Study to PP Counterparts. *J. Appl. Polym. Sci.* **2013**, *130*, 3175−3183.
(45) Scandola, M.; Ceccorulli, G.; Pizzoli, M. The Physical Aging of Bacterial Poly(D-β-hydroxybutyrate). *Macromol. Chem. Rapid Commun.* **1989**, *10*, 47−50.
(46) Thomas, S.; Zaikov, G. E. *Polymer Nanocomposites Research Advances*; Nova Science Publishers: New York, 2007; p 9.
(47) Tam, K. H.; Djurišić, A. B.; Chan, C. M. N.; Xi, Y. Y.; Tse, C. W.; Leung, Y. H.; Chan, W. K.; Leung, F. C. C.; Au, D. W. T. Antibacterial Activity of ZnO Nanorods Prepared by a Hydrothermal Method. *Thin Solid Films* **2008**, *516*, 6167−6174.
(48) Liu, H. L.; Yang, T. C. K. Photocatalytic Inactivation of Escherichia Coli and Lactobacillus Helveticus by ZnO and TiO_2 Activated with Ultraviolet Light. *Process Biochem.* **2003**, *39*, 475−481.
(49) Brayner, R.; Ferrari-Iliou, R.; Brivois, N.; Djediat, S.; Benedetti, M. F.; Fievet, F. Toxicological Impact Studies Based on Escherichia Coli Bacteria in Ultrafine ZnO Nanoparticles Colloidal Medium. *Nano Lett.* **2006**, *6*, 866−870.
(50) Heinlaan, M.; Ivask, A.; Blinova, I.; Dubourguier, H. C.; Kahru, A. Toxicity of Nanosized and Bulk ZnO, CuO and TiO2 to Bacteria Vibrio Fischeri and Crustaceans Daphnia Magna and Thamnocephalus Platyurus. *Chemosphere* **2008**, *71*, 1308−1316.
(51) Yamamoto, O. Influence of Particle Size on the Antibacterial Activity of Zinc Oxide. *Int. J. Inorganic Mater.* **2001**, *3*, 643−646.
(52) Ghule, K.; Ghule, A. V.; Chen, B.-J.; Ling, Y.-C. Preparation and Characterization of ZnO Nanoparticles Coated Paper and its Antibacterial Activity Study. *Green Chem.* **2006**, *8*, 1034−1041.
(53) Sanchez-Garcia, M. D.; Langaron, J. M.; Hoa, S. V. Effect of Addition of Carbon Nanofibers and Carbon Nanotubes on Properties of Thermoplastic Biopolymers. *Compos. Sci. Technol.* **2010**, *70*, 1095−1105.
(54) Sanchez-Garcia, M. D.; Langaron, J. M. Novel Clay-based Nanobiocomposites of Biopolyesters with Synergistic Barrier to UV Light, Gas, and Vapour. *J. Appl. Polym. Sci.* **2010**, *118*, 188−199.
(55) Fortunati, E.; Peltzer, M.; Armentano, I.; Torre, L.; Jiménez, C.; Kenny, J. M. Effects of Modified Cellulose Nanocrystals on the Barrier and Migration Properties of PLA Nano-biocomposites. *Carbohydr. Polym.* **2012**, *90*, 948−956.